

## Production Asymmetry Measurement of High $x_T$ Hadrons in $p\uparrow p$ -Collisions at 40 GeV

V.V.Abramov<sup>1</sup>, A.S.Dyshkant<sup>1</sup>, V.N.Evdokimov<sup>1</sup>, P.I.Goncharov<sup>1</sup>,  
A.M.Gorin<sup>1</sup>, A.N.Gurzhev<sup>1</sup>, Yu.P.Korneev<sup>1</sup>, A.V.Kostritskii<sup>1</sup>,  
A.N.KrinitSyn<sup>1</sup>, V.I.Kryshkin<sup>1</sup>, Yu.M.Mel'nik<sup>1</sup>, V.M.Podstavkov<sup>1</sup>,  
N.I.Sin'kin<sup>2</sup>, S.I.Tereshenko<sup>1</sup>, L.K.Turchanovich<sup>1</sup>, A.E.Yakutin<sup>1</sup>,  
A.A.Zaichenko<sup>1</sup>, V.N.Zapol'sky<sup>1</sup>

<sup>1</sup>Institute for High Energy Physics, Protvino, Russia

<sup>2</sup>Institute of Theoretical and Experimental Physics, Moscow, Russia

### Abstract

Single-spin asymmetries for hadrons have been measured in collisions of transversely-polarized 40 GeV/c proton beam with an unpolarized liquid hydrogen target. The asymmetries were measured for  $\pi^\pm$ ,  $K^\pm$ , protons and antiprotons, produced in the central region ( $0.02 \leq x_F \leq 0.10$  and  $0.7 \leq p_T \leq 3.4$  GeV/c). Asymmetries for  $\pi^\pm$ ,  $K^\pm$  and  $\bar{p}$  show within measurement errors the linear dependence on  $x_T$  and change a sign near 0.37. For protons negative asymmetry, independent of  $x_T$  has been found. The results are compared with those of other experiments and SU(6) model predictions.

Submitted to *Nucl. Phys. B*

# 1 Introduction

It is widely believed that the role of spin is decreasing with the rise of beam energy and transverse momentum ( $p_T$ ) of secondary particles. In particular, the perturbative QCD predicts the vanishing of spin effects with the rise of  $p_T$  [1]. Experiments performed during last years have shown much more complicated picture. It was found that polarization of  $\Lambda$ -hyperons produced in hadron-hadron collisions is almost energy independent and is rising with  $p_T$  and  $x_F = 2p_Z^*/\sqrt{s}$ , where  $p_Z^*$  and  $\sqrt{s}$  are, respectively, longitudinal momentum of secondary particle and total reaction energy in C.M. [2]. Single-spin asymmetry ( $A_N$ ) is rising with  $p_T$  and  $x_F$  at least for  $\pi^-$ - mesons and it differs from zero up to the highest available beam energies (200 GeV) [3], [4].

It seems, that the most promising among theoretical approaches to the solution of large single-spin asymmetry problem, observed in experiments, is to take into account higher twists contributions (see, for example [5]).

The existing data on single-spin asymmetries have in most cases, limited statistical accuracy,  $x_T = 2p_T/\sqrt{s}$  and  $x_F$  ranges as well as incomplete particle identification. That does not allow one to make definite conclusions about asymmetry dependence on kinematical variables and quantum numbers of hadrons.

The goal of the experiment is to study single-spin asymmetry ( $A_N$ ) in reactions:

$$p \uparrow + p(A) \rightarrow h + X, \quad (1)$$

where  $h$  denotes  $\pi^\pm$ ,  $K^\pm$ ,  $p$ ,  $\bar{p}$  or hadron pair [6].

It includes, in particular, the following points:

- $A_N$  vs  $x_T$  and  $x_F$  ( $x_T$  and  $x_F$  scaling check);
- $A_N$  vs quark flavor (u,d,s);
- $A_N$  vs A - atomic number (nature of A-dependence);
- $A_N$  vs  $x_T$  for hadron pairs.

The experiment has been carried out with FODS-2 double arm spectrometer designed to study high  $p_T$  single and pair hadron production in pp-,  $\pi$ p-, pA- and  $\pi$ A- collisions [7]. A new IHEP polarized 40 GeV/c proton beam gives an additional tool to study high  $p_T$  processes in reactions (1). The

beam energy and available intensity of polarized beam allow one to measure  $A_N$  in a wide  $x_F$  and  $x_T$  range ( $x_T < 0.9$ ) for not so high  $p_T$  (up to 3.4 GeV/c) of charged hadrons.

Preliminary results of this experiment, based on half the statistics, were reported at SPIN-95 workshop in Protvino [8].

## 2 Beam

Polarized protons [6] are produced via decays of  $\Lambda$ -hyperons. A slow extracted 70 GeV/c proton beam with intensity up to  $10^{13}$  ppp strikes the primary target. Charged particles, produced in the primary target, are deflected and absorbed in a beam dump. Protons from  $\Lambda$ -decays are collimated in vertical direction to select polarization sign and beam intensity. Average polarization of 40 GeV/c beam (for  $\Delta p/p = \pm 4.5\%$ ) is  $39_{-3}^{+1}\%$  and it was estimated using Monte Carlo simulation of the polarized beam production. The vertical beam position on the secondary target is corrected by two magnets. The beam polarization sign changes automatically each 15 minutes during 3-4 spills. Beam monitoring is performed by ionization chambers and scintillator monitors (arm triggers) with relative precision better than 1%. Calculated and measured beam parameters are in a good agreement, which gives us confidence in the knowledge of its polarization calculation.

## 3 Spectrometer

The experimental setup FODS-2 is a rotating double arm spectrometer [7] shown schematically in Fig.1. It includes a two gap magnet, drift chambers to measure momentum and angles of particles production, two Cerenkov ring imaging detectors (SCOCH) to identify particles, scintillation counters, hodoscopes and hadronic calorimeters to make trigger decision. The SCOCH detector is able to identify hadrons in the following momentum ( $p$ ) ranges:  $\pi^\pm$  ( $2 < p < 24$  GeV/c),  $K^\pm$  ( $4 < p < 24$  GeV/c), p and  $\bar{p}$  from 8 up to 24 GeV/c. Protons and antiprotons were also identified in the momentum range from 5 to 8 GeV/c using the absence of a signal in the SCOCH detector. The transverse position ( $X, Y$ ) of an interaction point in the hydrogen target ( $D=7$  cm,  $L=40$  cm,  $L/\lambda_{abs}=5\%$ ) is measured with beam hodoscopes.

Longitudinal coordinate ( $Z$ ) is determined as a result of matching  $X, Y$ -coordinates, measured with beam hodoscopes, with a particle trajectory, reconstructed using drift chambers downstream of the magnet. Hodoscopes resolution is  $\pm 1$  mm, both for  $X$  and  $Y$  coordinates. The total number of channels in each hodoscope plane is 32, and average multiplicity was around 2 per plane. When the multiplicity is not equal to unity a hodoscope channel closest to the center of gravity for the beam during the spill is used. Ionization chambers were used to determine the center of gravity for the beam.

## 4 Measurements

The measurements were carried out during 6 days of the November Run in 1994. The mean intensity of the polarized beam was  $9 \cdot 10^6$  ppp, limited by radiation environment. Now the shielding has been improved and nominal intensity up to  $2.6 \cdot 10^7$  can be achieved. The trigger for each arm required signals from the scintillation counters and energy deposition above threshold in the hadronic calorimeter. The total number of polarized protons that struck the target was about  $1.8 \cdot 10^{11}$  for each polarization sign. The corresponding number of recorded events is  $6.3 \cdot 10^5$ /polarization/arm. 24% of them have been reconstructed and identified for the final analysis.

## 5 Data reduction

The reconstructed trajectory of a particle downstream the spectrometer magnet is used to determine its momentum and production angles. Since the magnet deflects charged particles in vertical direction it does not change essentially polar angle ( $\theta$ ), but changes azimuthal angle ( $\phi$ ) depending on momentum and sign of the particle. The mean value of  $\cos\phi$  varies from 0.80 to 0.89.

Particle momentum was determined by matching incident particle transverse coordinates in the target ( $X, Y$ ), measured with the beam hodoscopes having the trajectory downstream the magnet. The momentum ( $p$ ) of hadron is used to determine its mass ( $m$ ):

$$m^2 = p^2(1 - \beta^2)/\beta^2, \quad (2)$$

where  $\beta$  is hadron velocity, measured with the SCOCH detector [9]. Mass spectrum ( $m^2$ ) of hadrons measured with the SCOCH is shown in Fig.2. For heavy hadrons (protons) the main error in  $m^2$  is due to the uncertainty in the momentum. For light particles ( $\pi$ -meson) the error in  $m^2$  is mainly due to the uncertainty in  $\beta$ .

## 6 Results

Single-spin asymmetry has been calculated for two arms ( $L$ -left,  $R$ -right):

$$A_N^L = \frac{1}{P_B \cdot \cos\phi} \cdot \frac{N_L^u - N_L^d}{N_L^u + N_L^d}, \quad (3)$$

$$A_N^R = \frac{-1}{P_B \cdot \cos\phi} \cdot \frac{N_R^u - N_R^d}{N_R^u + N_R^d}, \quad (4)$$

where  $P_B$  is the average beam polarization (39%), and  $N_{L(R)}^{u(d)}$  is the number of normalized events, for protons, polarized up ( $u$ ) or down ( $d$ ) for the left ( $L$ ) or right ( $R$ ) arm. The so called canonical helicity frame is used here for asymmetry definition, as it is in [3]. Asymmetries for two arms have been averaged, which decreased some systematic errors and doubled the statistics. Only statistical errors are taken into account in the results. The relative systematic error in  $A_N$  due to possible errors in beam polarization, beam monitoring and  $\cos\phi$  measurement is estimated to be less than 20%.

Along with the asymmetries for single particles the asymmetries for particle ratios have been calculated as well since they are free from beam monitoring problems.

Asymmetries for  $\pi^\pm$ ,  $K^\pm$ , protons and antiprotons are presented as functions of  $p_T$  in Table 1, 2 and 3, respectively. Asymmetry for  $\pi^+$  is shown in Fig.3, as a function of  $x_T$ . The lines in the figure represent fit by expression:

$$A_N = A_0(x_T - X_0), \quad (5)$$

where slope ( $A_0$ ) and sign change point ( $X_0$ ) are free parameters.

The bin width for  $p_T$  is 0.25 GeV/c and mean  $p_T$  varies from 0.66 to 3.37 GeV/c. The plotted values of  $x_T$  correspond to the mean values within the bins. Since the laboratory angle of the FODS-2 spectrometer is  $9^\circ$ , mean

Table 1:  $A_N$  vs  $p_T$  for  $\pi^+$  and  $\pi^-$  -mesons.

$p_T$ (GeV/c)	$A_N^{\pi^+}$	$A_N^{\pi^-}$
0.661	-0.12 $\pm$ 0.10	-0.017 $\pm$ 0.080
0.912	-0.085 $\pm$ 0.046	-0.040 $\pm$ 0.033
1.131	-0.018 $\pm$ 0.019	-0.005 $\pm$ 0.012
1.368	-0.027 $\pm$ 0.013	-0.020 $\pm$ 0.011
1.613	+0.009 $\pm$ 0.014	-0.037 $\pm$ 0.014
1.861	+0.002 $\pm$ 0.019	-0.018 $\pm$ 0.022
2.110	+0.035 $\pm$ 0.027	-0.027 $\pm$ 0.035
2.360	+0.091 $\pm$ 0.039	+0.068 $\pm$ 0.056
2.613	+0.065 $\pm$ 0.058	-0.062 $\pm$ 0.081
2.864	-0.012 $\pm$ 0.083	-0.05 $\pm$ 0.11
3.118	+0.20 $\pm$ 0.11	-0.24 $\pm$ 0.16
3.368	+0.21 $\pm$ 0.16	-0.21 $\pm$ 0.20

values of corresponding  $x_F$  at 40 GeV beam energy are not exactly zero and are rising from 0.02 to 0.10 with the rise of  $p_T$ . Asymmetry for  $\pi^+$  is rising with  $x_T$  and changes sign near  $x_T = 0.37$ .

The data for the BNL experiment [3] are also shown in Fig.3 for comparison. It is seen from Fig.3 that  $A_N$  changes sign at the same  $x_T$  for three different beam energies (13.3, 18.5 and 40 GeV). The cut  $x_F \leq 0.18$  is used for the BNL data to compare with this experiment.

Asymmetry for  $\pi^-$  is shown in Fig.4, where BNL data are also shown for comparison. Asymmetry for  $\pi^-$  is negative and it is rising in absolute value with  $x_T$  increase.  $A_N$  at the BNL energies is close to zero with some indication for positive slope  $A_0$ .

Table 2:  $A_N$  vs  $p_T$  for  $K^+$  and  $K^-$  -mesons.

$p_T$ (GeV/c)	$A_N^{K^+}$	$A_N^{K^-}$
0.661	$-0.60 \pm 0.46$	$+0.65 \pm 0.42$
0.912	$+0.01 \pm 0.15$	$+0.15 \pm 0.16$
1.131	$-0.074 \pm 0.049$	$-0.046 \pm 0.051$
1.368	$+0.011 \pm 0.029$	$+0.004 \pm 0.039$
1.613	$+0.005 \pm 0.030$	$-0.000 \pm 0.051$
1.861	$-0.016 \pm 0.038$	$+0.034 \pm 0.077$
2.110	$+0.135 \pm 0.052$	$+0.06 \pm 0.12$
2.360	$+0.056 \pm 0.075$	$+0.05 \pm 0.16$
2.613	$+0.03 \pm 0.11$	$+0.40 \pm 0.19$
2.864	$+0.10 \pm 0.15$	$+0.36 \pm 0.23$
3.118	$+0.33 \pm 0.18$	$+0.00 \pm 0.27$
3.368	$+0.28 \pm 0.23$	$+0.65 \pm 0.29$

Asymmetry for  $K^+$  (Fig.5) is rising with  $x_T$  similar to  $\pi^+$  data and changes sign at  $x_T$  near 0.37.

Asymmetries for  $K^-$  and antiprotons (Fig.5) have an indication of the rise with  $x_T$  similar to  $K^+$  data but statistical errors are too high to make this conclusion final. The last three points for  $\bar{p}$  from Table 3 are combined in Fig.5 to decrease error.

The comparison of  $A_N$  for protons with the BNL data are shown in Fig.6, as a function of  $x_T$ . For both experiments  $A_N$  does not depend on  $x_T$  and at 40 GeV the mean value of  $A_N$  is  $-0.050 \pm 0.009$ . The mean value of  $A_N$  within explored range of  $x_T$  is shown in Fig.7 for three energies as a function of  $\sqrt{s}$ . It is seen from Fig.7, that the mean value of  $A_N$  is well described by

Table 3:  $A_N$  vs  $p_T$  for protons and antiprotons.

$p_T$ (GeV/c)	$A_N^p$	$A_N^{\bar{p}}$
0.912	$-0.024 \pm 0.082$	$+0.44 \pm 0.20$
1.131	$-0.064 \pm 0.029$	$+0.017 \pm 0.067$
1.368	$-0.047 \pm 0.020$	$-0.023 \pm 0.068$
1.613	$-0.071 \pm 0.025$	$+0.09 \pm 0.12$
1.861	$-0.050 \pm 0.020$	$-0.17 \pm 0.17$
2.110	$-0.013 \pm 0.023$	$+0.08 \pm 0.22$
2.360	$-0.066 \pm 0.030$	$+0.19 \pm 0.29$
2.613	$-0.085 \pm 0.043$	$+0.02 \pm 0.34$
2.864	$-0.064 \pm 0.060$	$+1.06 \pm 0.37$
3.118	$-0.009 \pm 0.085$	$+0.44 \pm 0.41$
3.368	$+0.05 \pm 0.11$	$-0.21 \pm 0.47$

a linear function of  $\sqrt{s}$ :

$$A_N = (0.0113 \pm 0.0027)(4.34 \pm 0.45 - \sqrt{s}/GeV). \quad (6)$$

This result, if it is confirmed by other experiments, can be used to measure beam polarization in a wide range of energies.

As was mentioned above asymmetry for particle ratios, which under the first approximation equals the difference of asymmetries for two types of particles, is not sensitive to beam monitoring and thus has less systematics. Predictions of models in many cases are also better defined for particle ratios than for each particle separately. As an example of asymmetries for particle ratios Fig.8 shows  $A_N$  for  $K^+/\pi^+$  and  $K^-/\pi^-$  ratios. For  $K^+/\pi^+$ -ratio  $A_N$  is consistent with zero, as could be expected, since the fragmentation of



scattered valence  $u$ -quark is a main production source of both mesons [10]. Asymmetry for  $K^-/\pi^-$  is increasing with  $x_T$  and it is positive for  $x_T \geq 0.28$ .

Fit parameters for the data, shown in Figs. 3-8, are presented in Table 4. As is seen from Table 4 there is a significant slope ( $A_0$ ) in dependence on  $A_N$  vs  $x_T$  (5) for all particles except protons. The sign of the slope is positive for particles containing valence  $u$ -quark of colliding hadrons (for  $\pi^+$ ,  $K^+$ ), or sea quark (for  $K^-$ ,  $\bar{p}$ ). For particles containing valence  $d$ -quark from colliding hadrons (for  $\pi^-$ ) it is negative.

Table 4: Parameters  $X_0$  and  $A_0$  of equation (4) as a function of energy.

Ref.	hadron	E (GeV)	$X_0$	$A_0$
FODS-2	$\pi^+$	40.0	$0.37 \pm 0.02$	$0.33 \pm 0.08$
FODS-2	$\pi^-$	40.0	$0.06 \pm 0.19$	$-0.08 \pm 0.05$
FODS-2	$K^+$	40.0	$0.35 \pm 0.04$	$0.46 \pm 0.16$
FODS-2	$K^-$	40.0	$0.32 \pm 0.04$	$0.59 \pm 0.25$
FODS-2	$\bar{p}$	40.0	$0.24 \pm 0.12$	$0.43 \pm 0.39$
[3]	$\pi^+$	13.3	$0.33 \pm 0.04$	$0.33 \pm 0.11$
[3]	$\pi^+$	18.5	$0.37 \pm 0.02$	$0.58 \pm 0.14$
[3]	$\pi^-$	13.3	$0.018 \pm 0.024$	$0.037 \pm 0.019$
[3]	$\pi^-$	18.5	$0.007 \pm 0.005$	$0.025 \pm 0.026$
FODS-2	$K^+/\pi^+$	40.0	$0.27 \pm 0.23$	$0.11 \pm 0.17$
FODS-2	$K^-/\pi^-$	40.0	$0.29 \pm 0.04$	$0.70 \pm 0.26$

As was shown above, the asymmetry dependence on  $x_T$  can be described by linear function (5). To study the dependence of parameters  $A_0$  and  $X_0$  of (5) on energy we fitted  $x_T$  dependence of asymmetry for several experiments in a wide range of energies [3], [11], [12], [13]. Since in some experiments only  $\pi^0$ -mesons have been detected, their asymmetry is compared below with

mean  $A_N$  for  $\pi^+$  and  $\pi^-$ -mesons, averaged according to a parton model with weights proportional to their production cross sections [14]:

$$A_N(\pi^o) = \frac{A_N(\pi^+) \cdot R(x_T) + A_N(\pi^-)}{R(x_T) + 1}, \quad (7)$$

where  $R(x_T)$  is a ratio of the production cross sections for  $\pi^+$  and  $\pi^-$  - mesons. The resulting dependences of  $X_0$  and  $A_0$  on  $\sqrt{s}$  are shown in Figs.9-10, respectively. The dependence of  $X_0$  on  $\sqrt{s}$  is consistent with constant value of  $X_0 = 0.374 \pm 0.009$ , while  $A_0$  decreases with the rise of energy:

$$A_0 = (0.029 \pm 0.005) * (21 \pm 2 - \sqrt{s}/GeV), \quad (8)$$

which means the decrease of spin effects with the rise of energy. Scaling for  $X_0$ , observed in different experiments, proves that we have no significant systematics for asymmetry in this experiment. One point in Fig.10, corresponding to the PROZA-M experiment result is much higher than other points, which could be related to different beam ( $\pi^-$ ) for that experiment [11]. Of course, the exact dependence of  $A_0$  on energy is unavailable and the linear expression is just the simplest one.

It is interesting to compare the observed scaling for parameter  $X_0$  with predictions of theoretical models. Predictions for asymmetry in the central region for a wide range of energies have been recently made in the framework of QCD [14]. The main role in this model belongs to the orbital angular momentum of the quark-antiquark cloud in the internal structure of constituent quarks. For polarization of the constituent quarks SU(6)-model values  $P_U = 2/3$  and  $P_D = -1/3$  are used. Predictions of asymmetry for  $\pi^+$  and  $\pi^-$ -mesons have been made for 70, 200 and 800 GeV. These predictions along with their extrapolation to 40 GeV are shown in Fig.11 as the functions of  $x_T$ . It is seen from Fig.11, that the value of  $x_T$ , where  $A_N = 0$  is decreasing with the energy rise (which corresponds to constant  $p_T = 0.75$  GeV/c), contrary to the experimental data where it takes place at constant  $x_T$  around 0.37.

The comparison of data and model predictions for 40 GeV is shown in Fig.12. The 40 GeV energy model predictions are in a qualitative agreement with the results of this experiment. The model predicts the rise of  $A_N$  with  $x_T$ , the opposite sign of  $A_N$  for  $\pi^+$  and  $\pi^-$ , and half as much the absolute value of asymmetry for  $\pi^-$  against for  $\pi^+$ . The model predicts the increase for  $A_0$  and the decrease for  $X_0$  with the rise of energy. That is in some

contradiction with the results shown in Figs.9-10 for  $\pi^0$ -mesons. Asymmetry for  $\pi^0$ -meson at 200 GeV is very small [13], which is possible to explain if  $P_U = -P_D$  and hence  $A_N^{\pi^+} = -A_N^{\pi^-}$ , which is not seen at 40 GeV energy and below it.

## 7 Conclusion

The first asymmetry measurements have been performed for  $\pi^\pm$ ,  $K^\pm$ , p and  $\bar{p}$  with 40 GeV/c IHEP polarized proton beam. Asymmetries for  $K^\pm$  and  $\bar{p}$  have never been measured before. Asymmetries for  $\pi^\pm$ ,  $K^\pm$ ,  $\bar{p}$  show approximately linear dependence on  $x_T$  and change the sign near 0.37. The slope sign of this dependence is negative for  $\pi^-$  and positive for other hadrons, except protons. For protons the negative asymmetry, independent of  $x_T$  has been found, which grows with energy in absolute value as the comparison with the other experiment indicates.

The SU(6) model predicts asymmetry that is in a qualitative agreement with our data for  $\pi$ -mesons.

A significant increase in statistics is possible (by a factor around 40) in future runs which will allow us to make definite conclusion about asymmetries in a wide range of  $x_T$  and  $x_F$ .

We gratefully acknowledge the assistance and support of the IHEP staff and directorate. The research was supported in part by the Russian Fund for Fundamental Research.

## References

- [1] G.Kane, J.Pumpkin, and W.Repko, Phys.Rev.Lett. 41(1978)1698.
- [2] G.Bunce et al., Phys. Rev. Lett. 36(1976)1113;  
L.Pondrom, Phys. Rep. 122(1985)57;  
J.Duryea et al., Phys.Rev. Lett. 67(1991)1193;  
A.Morelos et al., Phys. Rev. Lett. 71(1993)2172.
- [3] E.S.Saroff et al., Phys.Rev.Lett. 64(1990)995.
- [4] D.L.Adams et al., Z.Phys. C56(1992)181.
- [5] A.V.Efremov, V.M.Korotkiyan and O.V.Teryaev, Phys. Rep. 261(1995)N1,2.
- [6] A.S.Dyshkant et al., - In Proc. of the 5th Workshop on High Energy Spin Physics, Protvino, 1993, edited by S.B.Nurushev and L.F.Soloviev (Protvino, Russia, 1994), p.434
- [7] V.V.Abramov et al., PTE, 1992, N6, p.75; IHEP preprint 91-144, Protvino (1991).
- [8] V.V.Abramov et al., - In Proc. of the 6th Workshop on High Energy Spin Physics, Protvino, 1995, edited by S.B.Nurushev and Yu.V.Kharlov, (Protvino, Russia, 1996), Vol.2, p.51.
- [9] V.V.Abramov et al., Nucl. Instr. and Meth. A235(1985)497.
- [10] V.V.Abramov et al., Yad. Fiz. 41(1985)700.
- [11] V.D.Apokin et al., Phys.Lett. B243(1990)461.
- [12] J.Antille et al., Phys.Lett. B94(1980)523.
- [13] D.L.Adams et al., IHEP preprint 94-88, Protvino (1994).
- [14] S.M.Troshin and N.E.Tyurin, Phys.Rev. D52(1995)3862.

## List of Figures

1	The schematic layout of FODS-2 spectrometer. . . . .	14
2	Mass spectrum of hadrons measured by SCOCH detector. . . . .	15
3	Comparison of $A_N$ vs $x_T$ for $\pi^+$ -mesons at 40 GeV, 18.5 and 13.3 GeV [3]. Solid line shows fit (5) for 40 GeV, dashed line - for 13.3 GeV, and dotted line - for 18.5 GeV. . . . .	16
4	Comparison of $A_N$ vs $x_T$ for $\pi^-$ -mesons at 40 GeV, 18.5 and 13.3 GeV [3]. Solid line shows fit (5) for 40 GeV, dashed line - for 13.3 GeV, and dotted line - for 18.5 GeV. . . . .	17
5	Single-spin asymmetry vs $x_T$ for $K^+$ , $K^-$ -mesons and antiprotons. Solid line shows fit (5) for $K^+$ , dashed line - for $K^-$ , and dotted line - for antiprotons. . . . .	18
6	Comparison of $A_N$ vs $x_T$ for protons at 40 GeV, 18.5 and 13.3 GeV [3]. Solid line shows fit (5) for 40 GeV, dashed line - for 13.3 GeV, and dotted line - for 18.5 GeV. . . . .	19
7	$A_N$ vs CM collision energy for protons for FODS-2 and BNL [3] data. . . . .	20
8	Asymmetry vs $x_T$ for particle ratios $K^+/\pi^+$ and $K^-/\pi^-$ . Solid line shows fit (5) for $K^+/\pi^+$ , dashed line - for $K^-/\pi^-$ . . . . .	21
9	Dependence of parameter $X_0$ of eq. (5) vs CM collision energy for $\pi^0$ [11,12,13] and $\pi^+\pi^-$ [3], FODS-2. Asymmetries for $\pi^+$ and $\pi^-$ are added with weights proportional to the production cross sections for these mesons following (7). . . . .	22
10	Dependence of parameter $A_0$ of eq. (5) vs CM collision energy for $\pi^0$ [11,12,13] and $\pi^+\pi^-$ [3], FODS-2. Asymmetries for $\pi^+$ and $\pi^-$ are added with weights proportional to the production cross sections for these mesons following (7). . . . .	23
11	SU(6) model predictions of $A_N$ vs $x_T$ for $\pi^+$ and $\pi^-$ -mesons at different energies [14]. . . . .	24
12	Comparison of data and SU(6) model [14] predictions at 40 GeV. Data ( $A_N$ vs $x_T$ ) are shown for $\pi^+$ and $\pi^-$ -mesons. Predictions are shown by dotted curve ( $\pi^+$ ) and by dash-dotted curve ( $\pi^-$ ). . . . .	25

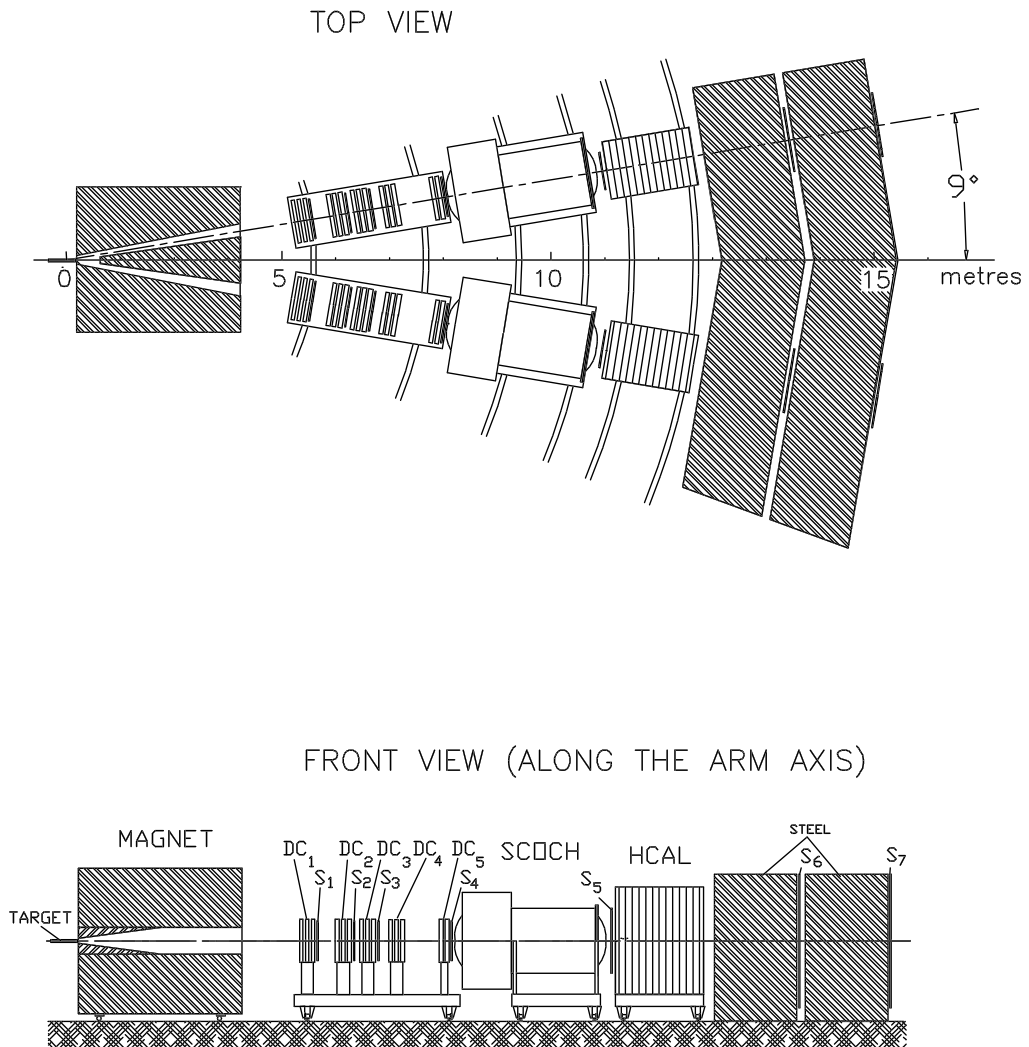


Figure 1: The schematic layout of FODS-2 spectrometer.

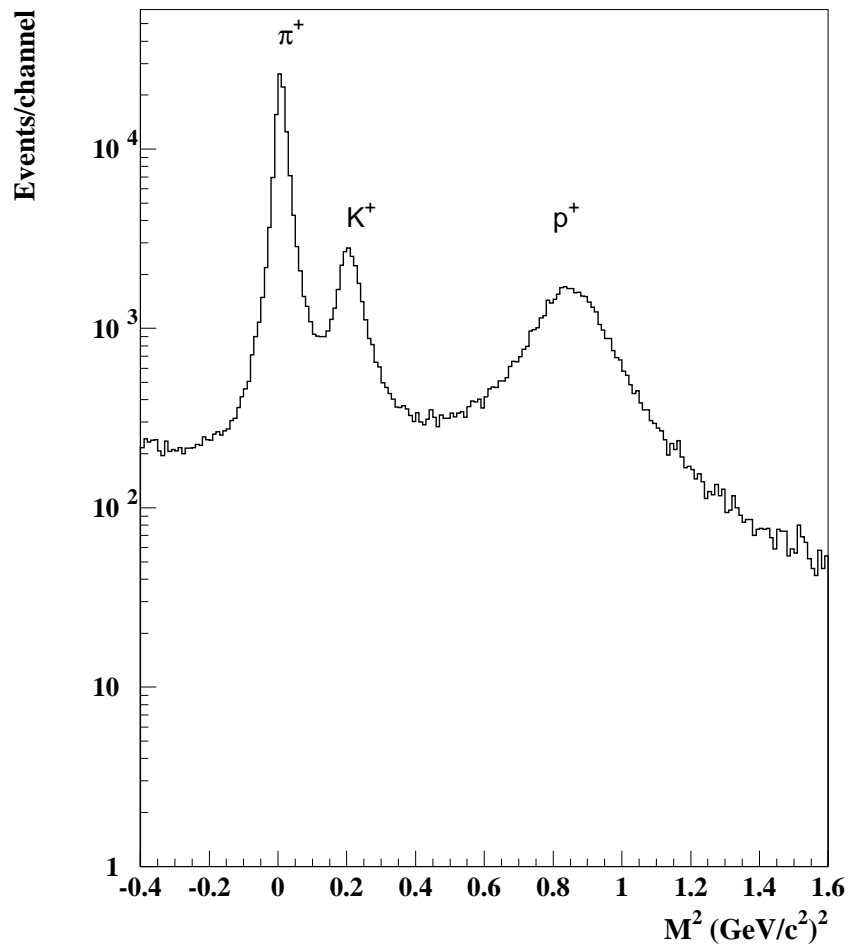


Figure 2: Mass spectrum of hadrons measured by SCOCH detector.

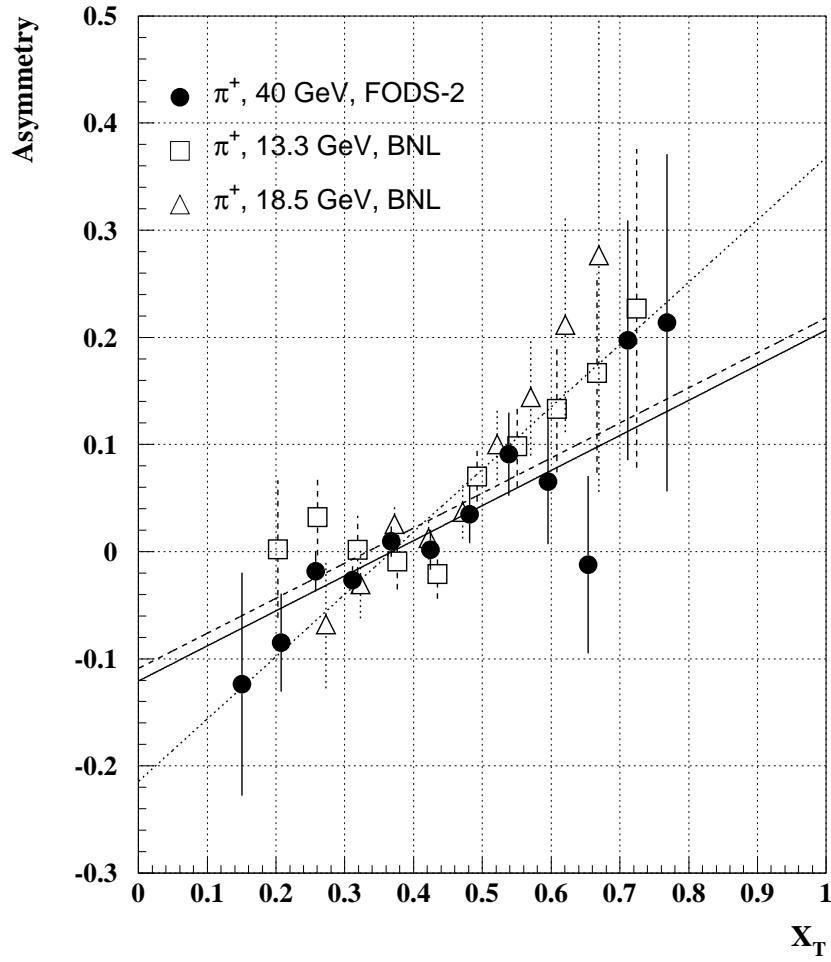


Figure 3: Comparison of  $A_N$  vs  $x_T$  for  $\pi^+$  -mesons at 40 GeV, 18.5 and 13.3 GeV [3]. Solid line shows fit (5) for 40 GeV, dashed line - for 13.3 GeV, and dotted line - for 18.5 GeV.



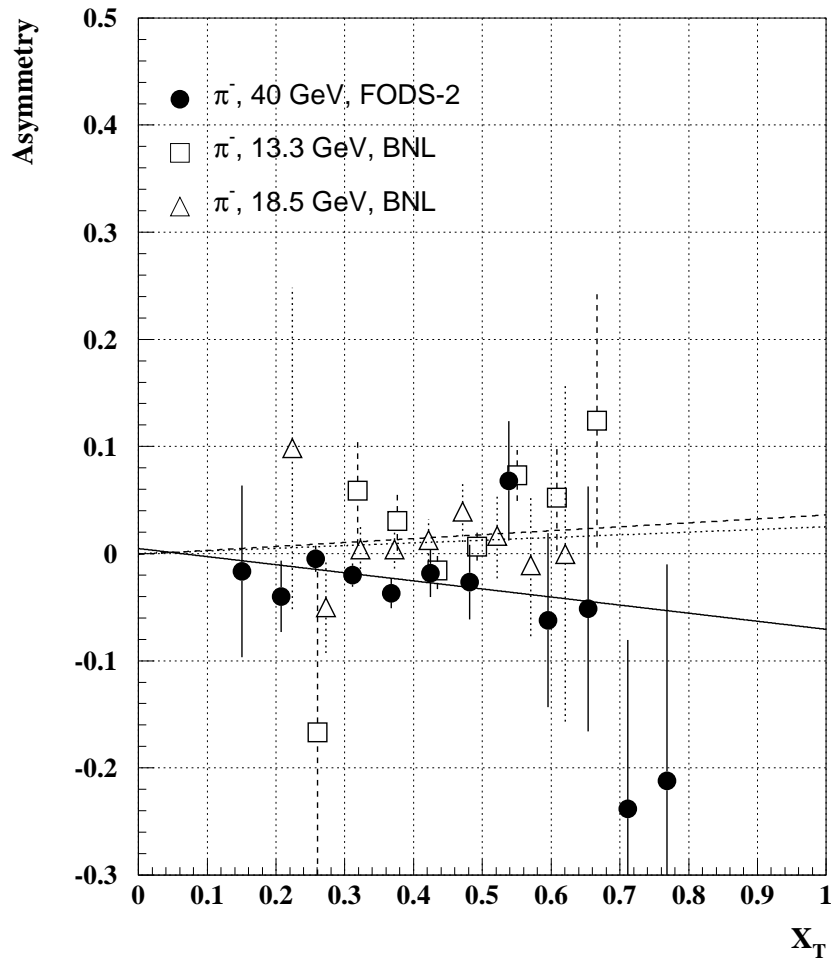


Figure 4: Comparison of  $A_N$  vs  $x_T$  for  $\pi^-$  -mesons at 40 GeV, 18.5 and 13.3 GeV [3]. Solid line shows fit (5) for 40 GeV, dashed line - for 13.3 GeV, and dotted line - for 18.5 GeV.

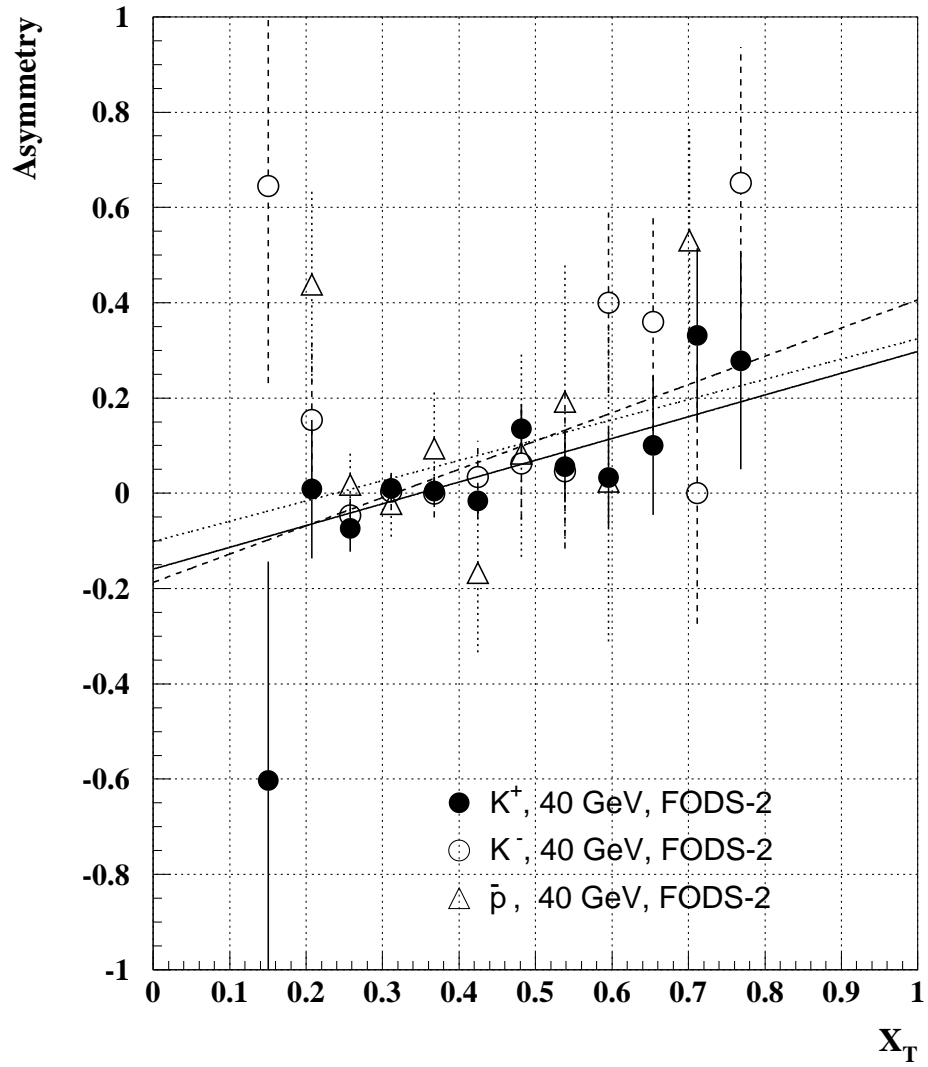


Figure 5: Single-spin asymmetry vs  $x_T$  for  $K^+$ ,  $K^-$  -mesons and antiprotons. Solid line shows fit (5) for  $K^+$ , dashed line - for  $K^-$ , and dotted line - for antiprotons.

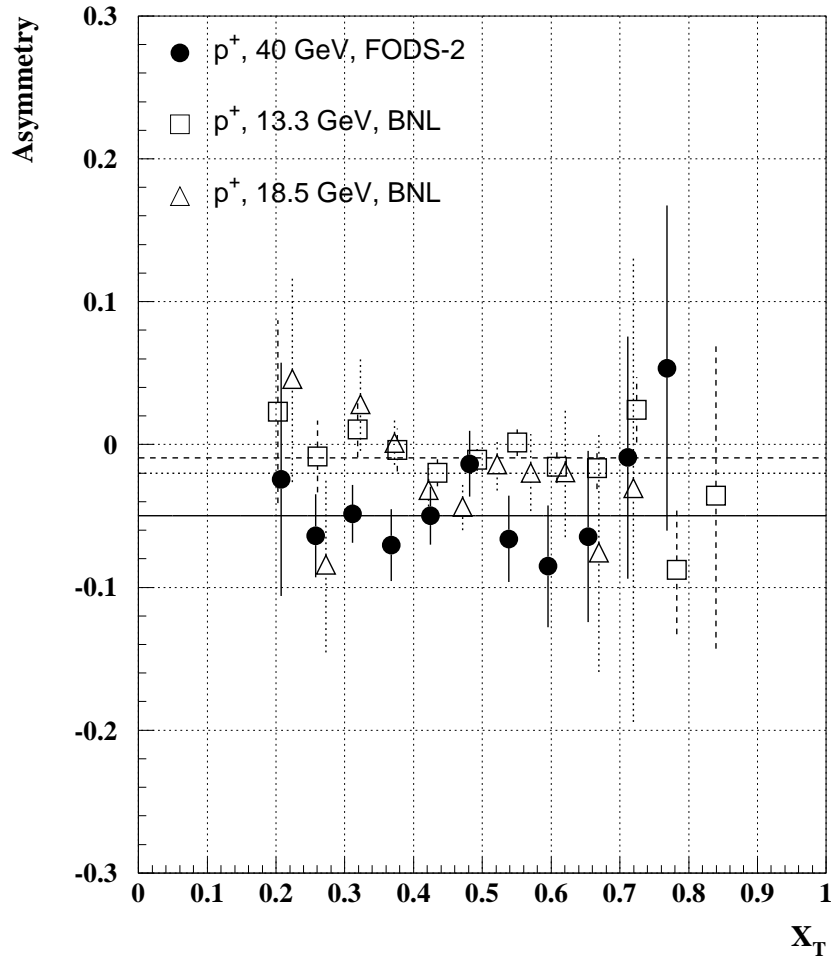


Figure 6: Comparison of  $A_N$  vs  $x_T$  for protons at 40 GeV, 18.5 and 13.3 GeV [3]. Solid line shows fit (5) for 40 GeV, dashed line - for 13.3 GeV, and dotted line - for 18.5 GeV.

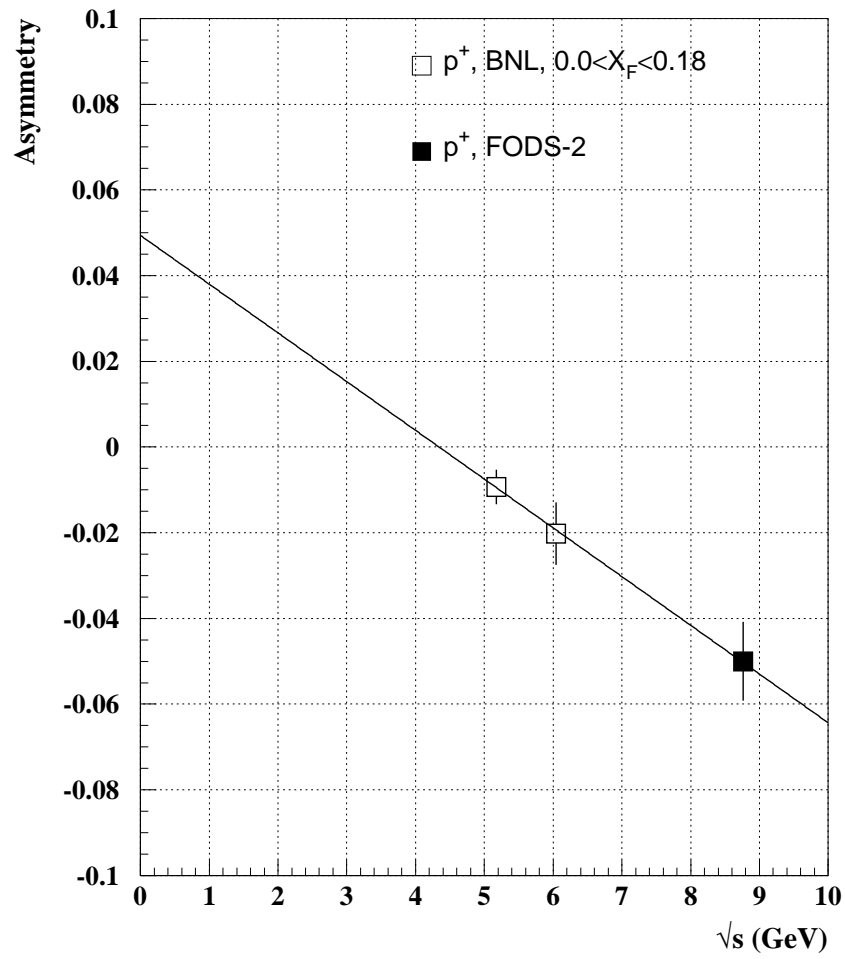


Figure 7:  $A_N$  vs CM collision energy for protons for FODS-2 and BNL [3] data.

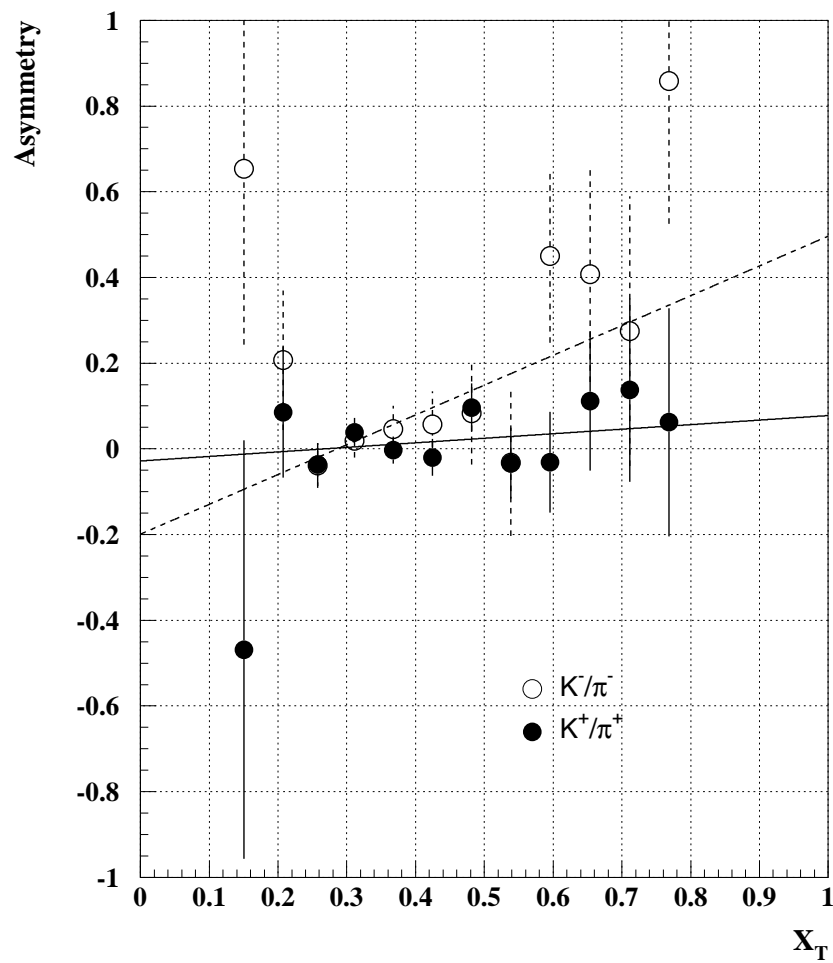


Figure 8: Asymmetry vs  $x_T$  for particle ratios  $K^+/\pi^+$  and  $K^-/\pi^-$ . Solid line shows fit (5) for  $K^+/\pi^+$ , dashed line - for  $K^-/\pi^-$ .

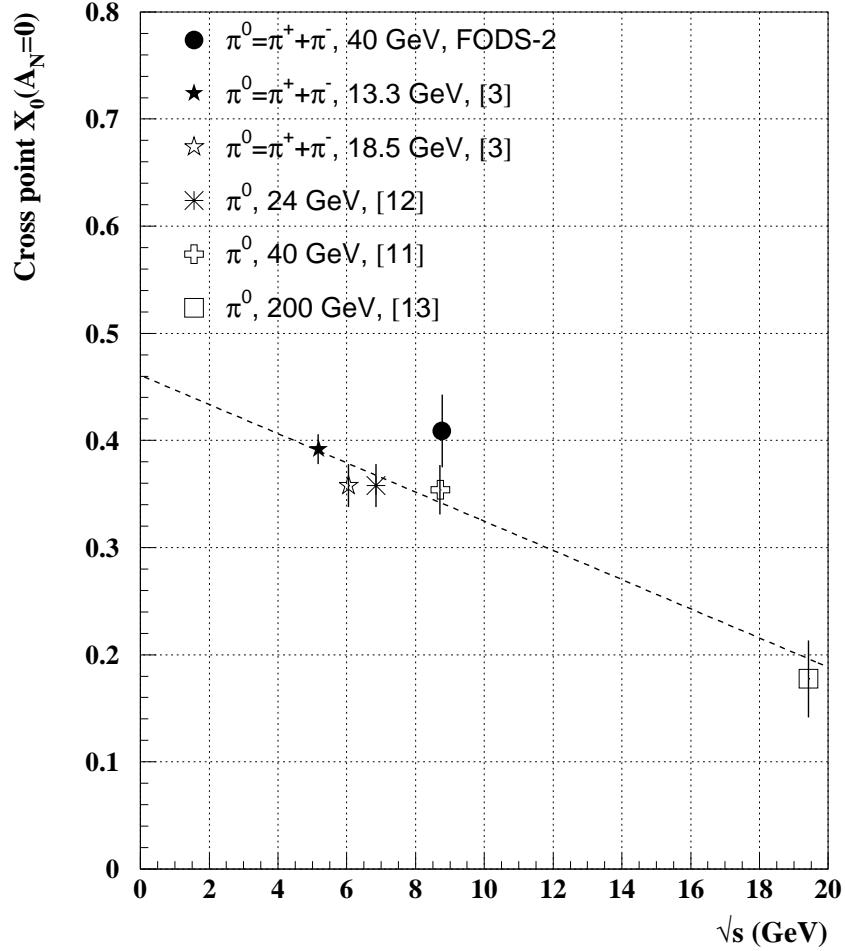


Figure 9: Dependence of parameter  $X_0$  of eq. (5) vs CM collision energy for  $\pi^0$  [11,12,13] and  $\pi^+ + \pi^-$  [3], FODS-2. Asymmetries for  $\pi^+$  and  $\pi^-$  are added with weights proportional to the production cross sections for these mesons following (7).

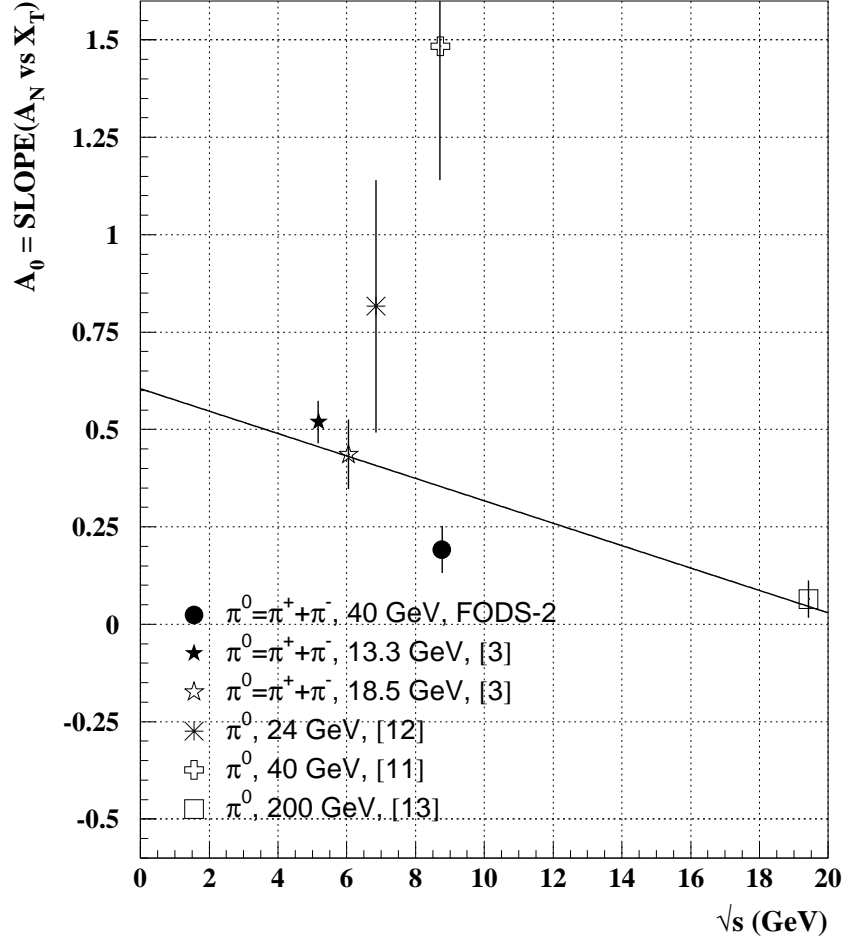


Figure 10: Dependence of parameter  $A_0$  of eq. (5) vs CM collision energy for  $\pi^0$  [11,12,13] and  $\pi^+ + \pi^-$  [3], FODS-2. Asymmetries for  $\pi^+$  and  $\pi^-$  are added with weights proportional to the production cross sections for these mesons following (7).

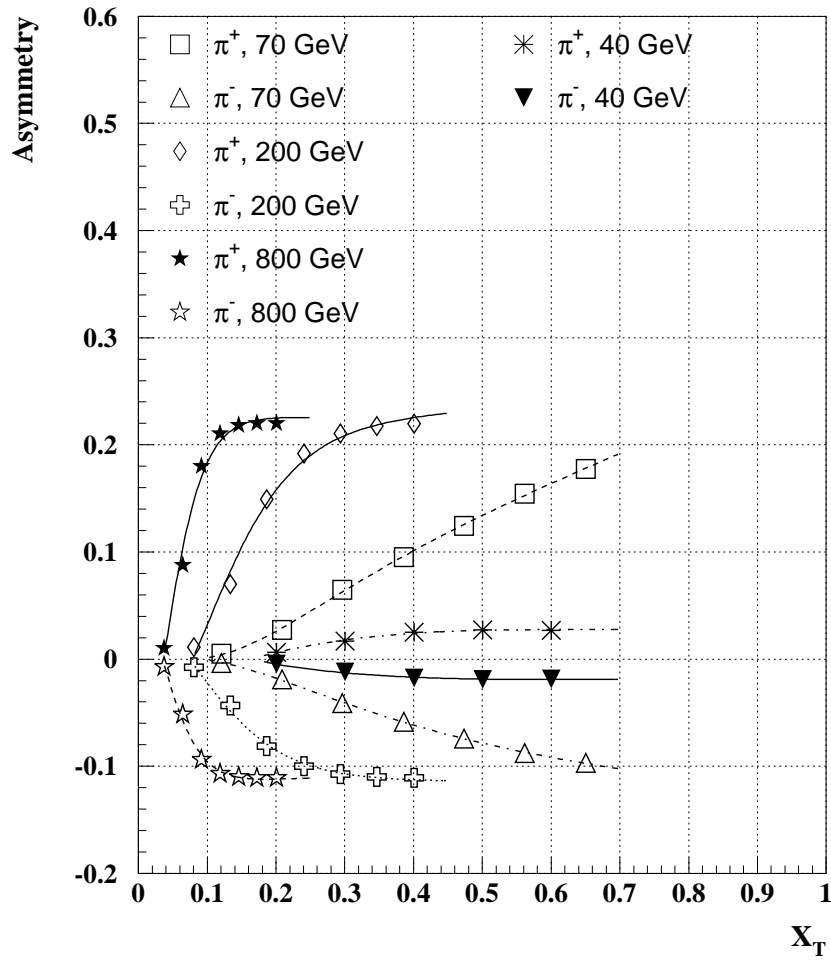


Figure 11: SU(6) model predictions of  $A_N$  vs  $x_T$  for  $\pi^+$  and  $\pi^-$  -mesons at different energies [14].



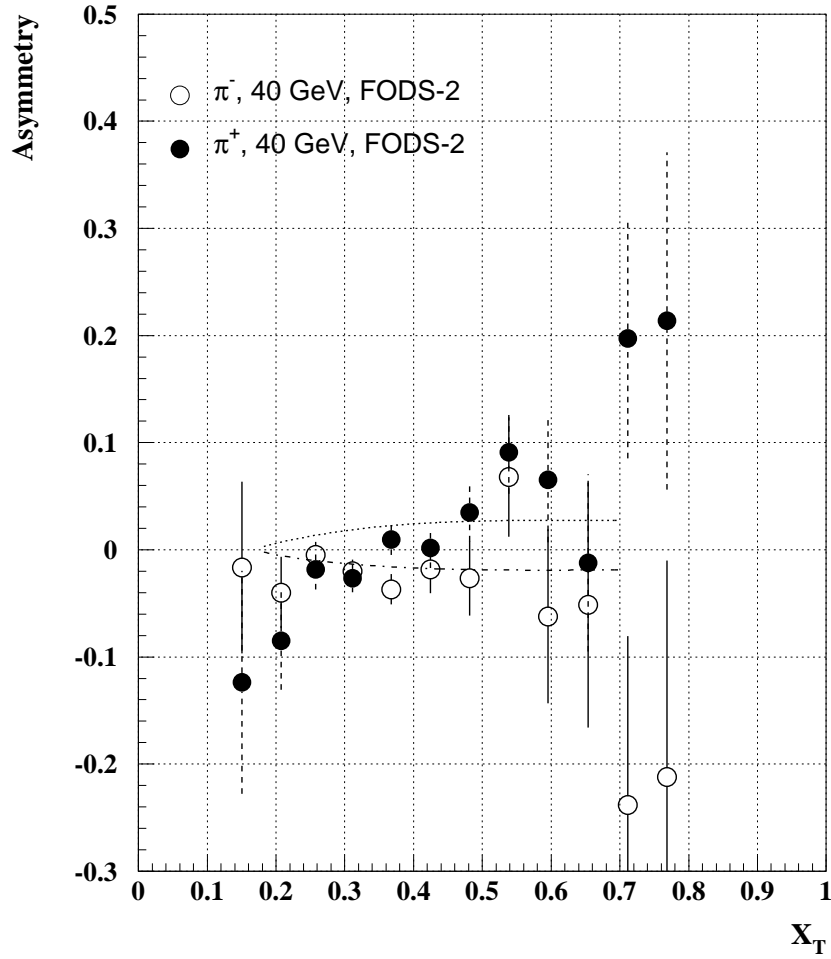


Figure 12: Comparison of data and SU(6) model [14] predictions at 40 GeV. Data ( $A_N$  vs  $x_T$ ) are shown for  $\pi^+$  and  $\pi^-$  -mesons. Predictions are shown by dotted curve ( $\pi^+$ ) and by dash-dotted curve ( $\pi^-$ ).